Chemical Bonding of the Binary Indium Bromides

Richard Dronskowski

Max-Planck-Institut für Festkörperforschung, Heisenbergstrasse 1, 70 569 Stuttgart, Germany

Received December 29, 1993[⊗]

In order to understand the chemical bonding of the binary indium bromides, we have performed both classical and quantum mechanical studies on all five crystallographically characterized phases (InBr, In_5Br_7, In_2Br_3, $InBr_2$, and $InBr_3$). Using a bond length−bond strength *Ansatz*, the different oxidation states of indium can be satisfactorily described by taking 266.7, 242.0, and 240.3 pm as standard bond distances r_0 for In^+-Br^-, $In^{2+}-Br^-$, and $In^{3+}-Br^-$ interactions. On the basis of charge-self-consistent semiempirical band structure calculations, it is argued that the reduced phases (InBr, In_2Br_3, and In_5Br_7) are "soft" and easy to perturb upon chemical reaction (in the spirit of Pearson's HSAB concept). Because of their electrophilicity, In_2Br_3 and In_5Br_7 may serve usefully as slightly acidic melts. Although coordination polyhedra around In^+ ions are highly irregular because of the influence of the almost doubly filled indium 5s atomic orbital, the total In^+-Br^- bonding interaction is similarly weak in all cases, and the crystal potential around In^+ seems to be very soft. In none of the cases, however, has there been found a *directed* electron "lone-pair" effect for In^+. While In^+-Br^- bonds are characterized by antibonding contributions at the frontier bands (out-of-phase combination between indium 5s and bromine 4p orbitals), true In−In interactions can be found in the case of the $In_2Br_6^{2-}$ species ($In^{2+}-In^{2+}$ single bond) and in the structure of InBr, here playing a stabilizing role for the unusual 7-fold coordination geometry. Judging from energetic considerations, the probability of In^+-In^+ partial bonds as centric defects inside an otherwise acentric In_2Br_3 crystal structure is nonzero but small.

1. Introduction

Indium is able to form a multitude of binary halides. Among these, the structural chemistry of the bromides is richest. There are five well-characterized indium bromides, namely InBr,[1] In_5Br_7 (≡$InBr_{1.4}$),[1,2] In_2Br_3 (≡$InBr_{1.5}$),[1,3] $InBr_2$,[1,4] and $InBr_3$,[1] while the existence of another possible phase, In_4Br_7 (≡$InBr_{1.75}$),[5,6] is still an open question. The astonishing structural variety can be traced back to the indium atom's multivalency (In^+, In^{2+}, and In^{3+}) and the possibility for mixing these valencies in varying combinations in the solid state.

We have investigated these compounds by means of charge-self-consistent semiempirical band structure calculations in order to elucidate the common bonding principles. Specifically, we were interested in the reason for the monovalent indium ion's coordination polyhedra being strongly irregular and in the possible existence of a *directed*, stereoactive electron "lone-pair" on In^+. The latter should show up as a sharp and local nonbonding (or almost nonbonding) contribution to the total electronic structure. As will be seen in the following, there are no obvious ties between traditional ideas of electron pair bond formation and the coordination polyhedra present. Similarly, no easy interpretation of the electronic structure by means of MO splittings (due to point group symmetry) is apparent at first sight—therefore the need for a systematic computational and numerical analysis.

2. Structural Chemistry

Instructive descriptions of the phases have been published in the original structure reports by Staffel and Meyer, by Beck, and by Bärnighausen;[1-4] the reader is referred to these for further information. In simple terms, the structures (especially the larger ones) of the binary indium bromides may be regarded as complicated packings of irregular coordination polyhedra. In order to guide the reader most conveniently, we will now focus on a short coherent structural inspection, *with a special emphasis on the indium ions and their bromine coordination*, in order of increasing complexity. All atomic labels correspond to the original papers and are also given in the supplementary material.

The simplest structure is present for monoclinic $InBr_3$ (*C2/m*: $a = 669.6$ pm, $b = 1164.1$ pm, $c = 663.3$ pm, $\beta = 108.99°$; $Z = 4$) which crystallizes in the $AlCl_3/YCl_3$ structure type. Here one finds one symmetry-independent In^{3+} ion, octahedrally coordinated by Br^- ions with a mean distance of 267 pm.

Another In^{3+} ion is present in orthorhombic $InBr_2$ (*Pnna*: $a = 798.6$ pm, $b = 1038.5$ pm, $c = 1042.5$ pm; $Z = 8$), isotypic with $GaCl_2$. In this case, however, the In^{3+} ion is tetrahedrally coordinated by Br^- ions with a mean distance of 250 pm. Since $InBr_2$ is a mixed In(I)−In(III) bromide according to $In^+In^{3+}(Br^-)_4$, there is also an In^+ ion in an almost cubelike 8-fold coordination by Br^- ions with a mean In^+-Br^- distance of 345 pm (Figure 1).

An even more peculiar coordination of an In^+ ion can be seen in the structure of orthorhombic InBr (*Cmcm*: $a = 446.6$ pm, $b = 1236.8$ pm, $c = 473.9$ pm; $Z = 4$), belonging to the TlI structure type. Now In^+ is seven-coordinated by Br^- ions with a mean distance of 342 pm. Figure 2 shows two of these connected coordination polyhedra, giving rise to a comparatively short In^+-In^+ distance of 355 pm.

For orthorhombic In_2Br_3, there are two competing structural descriptions available. The one published first[1] focuses on a *centric* unit cell (*Pnma*: $a = 1300.6$ pm, $b = 1649.8$ pm, $c = 1289.7$ pm; $Z = 16$) and states that In_2Br_3 crystallizes in the

[⊗] Abstract published in *Advance ACS Abstracts,* November 15, 1994.

(1) Staffel, T.; Meyer, G. *Z. Anorg. Allg. Chem.* **1987**, *552*, 113; **1988**, *563*, 27. Although a gap in In^+-Br^- distances seems to lie around 450 pm, the calculation of an *effective* coordination number (ECoN) for In^+ ions yielded values between 4.75 and 6.86.
(2) Marsh, R. E.; Meyer, G. *Z. Anorg. Allg. Chem.* **1990**, *582*, 128.
(3) Bärnighausen, H. *Z. Kristallogr.* **1989**, *186*, 16.
(4) Beck, H. P. *Z. Naturforsch.* **1987**, *42B*, 251.
(5) Walter, P. H. L.; Kleinberg, J.; Griswold, E. *J. Inorg. Nucl. Chem.* **1961**, *19*, 223.
(6) Morawietz, W.; Morawietz, H.; Brauer, G. *Z. Anorg. Allg. Chem.* **1962**, *316*, 220.

0020-1669/94/1333-6201$04.50/0

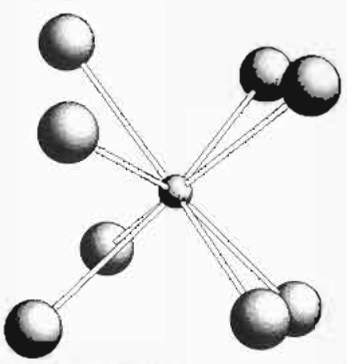

Figure 1. Coordination of In^+ by Br^- (up to 450 pm) within $InBr_2$. The almost cubic polyhedron is slightly distorted with respect to a square antiprism. The view direction is close to [100].

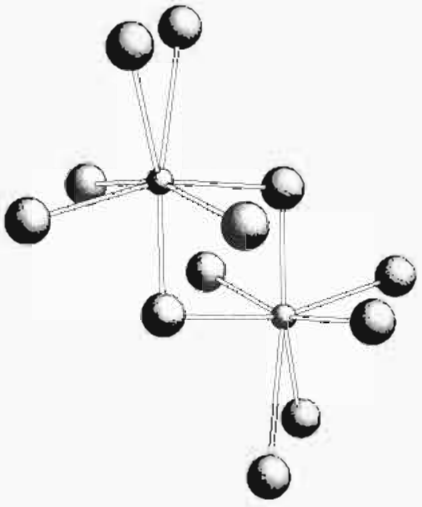

Figure 2. Coordination of In^+ by Br^- (up to 450 pm) within InBr. The view direction is close to [100].

Ga_2Br_3 structure type, following the valence composition $(In^+)_2(In^{2+})_2(Br^-)_6$. The second one[3] is based on a low-temperature investigation and takes advantage of an *acentric* space group ($P2_12_12_1$: a = 1293.8 pm, b = 1639.9 pm, c = 1285.5 pm at −60 °C; Z = 16). By use of bond length considerations, it is obvious that both descriptions are *almost equivalent*, especially when it comes to the connectivity between indium and bromine ions.[7]

Quite independent from the mode of description (for simplicity, we will from now on refer to the more compact centric characterization), there are three different In^+ coordination polyhedra. By restricting the range of In^+-Br^- interactions to distances less than 450 pm, one observes the In(4) ion to have an 8 + 1 coordination (monocapped cube; see Figure 3) with 362 pm as its mean bond distance. The monovalent In(5) ion has a 2 + 4 + 2 coordination with four Br^- ions almost in a plane (see Figure 4), the mean bond distance being 349 pm. Finally, the coordination of monovalent In(6) (see Figure 5) resembles very much the 8 + 1 scenario of In(4), the bromine cube having changed into a square antiprism, with an average In^+-Br^- bond distance of 357 pm.[8]

The divalent In^{2+} ions within In_2Br_3, on the other hand, are bonded within the dimeric species $In_2Br_6^{2-}$ with eclipsed

(7) The main difference, elaborated in section 4.5.1, lies in an additional splitting of two non-fully occupied In^+ ions of the centric description into four nonequivalent In^+ ions in the acentric case.

(8) Note that, because of charge neutrality, some In^+ sites can only be partially occupied. These are In(5) and In(6) on the 8d site with 75% occupation. This assignment is slightly changed in the acentric description (section 4.5.1).

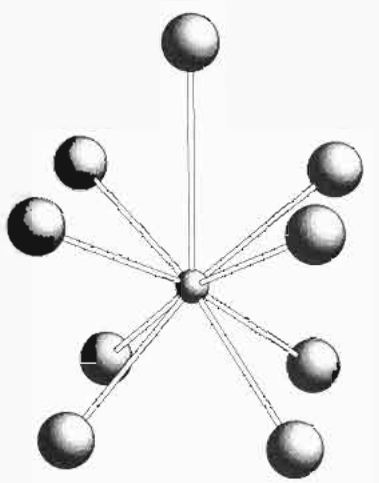

Figure 3. Coordination of monovalent In(4) by Br^- (up to 450 pm) within In_2Br_3 (centric description). The view direction is close to [100].

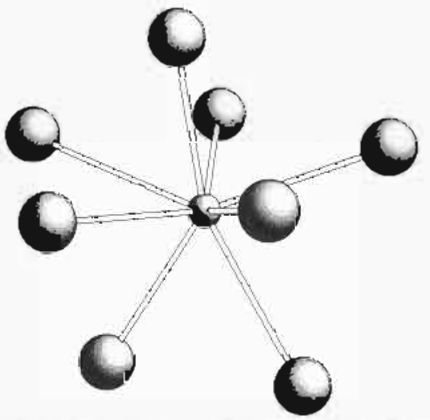

Figure 4. Coordination of monovalent In(5) by Br^- (up to 450 pm) within In_2Br_3 (centric description). The view direction is close to [001].

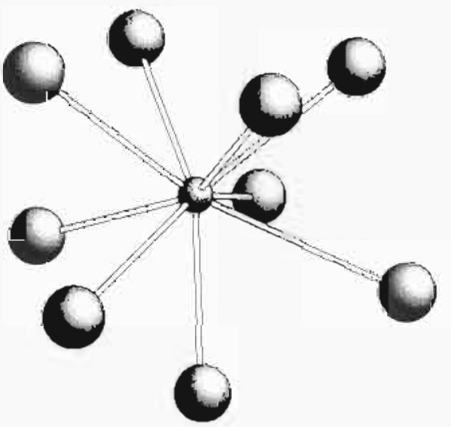

Figure 5. Coordination of monovalent In(6) by Br^- (up to 450 pm) within In_2Br_3 (centric description). The view direction is close to [010].

conformation, depicted in Figure 6. Thus, each In^{2+} ion is threefold coordinated by Br^- ions, with a mean distance of 257 pm, the other In^{2+} ion augmenting the coordination geometry via an $In^{2+}-In^{2+}$ single bond (270 pm distance) to form a distorted tetrahedron.

The most complex structure is the one of monoclinic In_5Br_7 ($C2/c$: a = 1868.8 pm, b = 1860.2 pm, c = 1921.7 pm, β = 104.19°; Z = 16) which is formally best described by $(In^+)_3(In^{2+})_2(Br^-)_7$, also containing dimeric species $In_2Br_6^{2-}$ exactly like in In_2Br_3. Somewhat simplified, two groups can be distinguished among the seven symmetry-independent In^+ ions: Ninefold coordination (2 + 4 + 3), with four Br^- ions

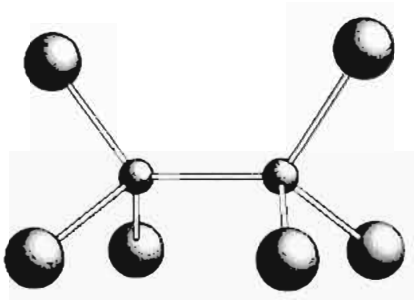

Figure 6. Dimeric species containing In^{2+} ions within In_2Br_3. The view direction is close to [010].

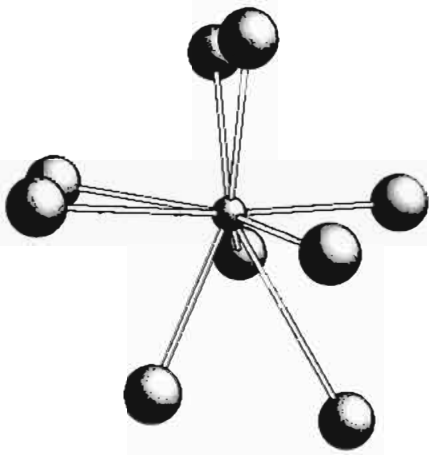

Figure 7. Coordination of monovalent In(1) (and approximately of In(2−4)) by Br^- (up to 450 pm) within In_5Br_7. The view direction is close to [100].

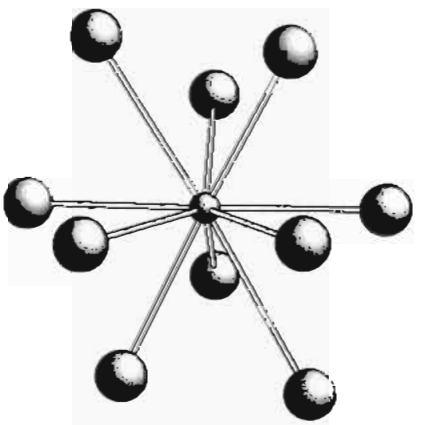

Figure 8. Coordination of monovalent In(7) (and approximately of In(5) and In(6)) by Br^- (up to 450 pm) within In_5Br_7. The view direction is close to [010].

almost in a plane (Figure 7), is found for In(1−4), with average bond distances between 358 and 359 pm. Tenfold coordination (3 + 4 + 3), also with four nearly coplanar Br^- ions (Figure 8), is present for In(5−7), with mean bond distances of 366−367 pm. This grouping is admittedly idealized, but some artificiality can never be excluded in any such description.

3. Theory

3.1. Bond Length−Bond Strength Considerations. The irregularities in coordination polyhedra around In^+ ions prevent a straightforward comparison of In^+-Br^- distances, and even a naive count of coordination numbers has proven to be rather difficult for In^+ ions.[1] The derivation of bond length−bond strength parameters for In^+, In^{2+}, and In^{3+} ions seems to be more promising. According to an empirical bond length−bond strength formula,[9] the bond strength s in valence units is given by

$$s = \exp\left(\frac{r_0 - r}{37\ \text{pm}}\right) \tag{1}$$

with r as the real bond distance and r_0 as a fixed scaling distance, whereas the atomic valence v is identical to the sum of all bond strengths:

$$v = \sum_i s_i \tag{2}$$

A systematic computerized refinement of above equations, based on 107 In^+-Br^- distances, 21 $In^{2+}-Br^-$ distances, and 10 $In^{3+}-Br^-$ distances, all of them from above structures (excluding the low-temperature In_2Br_3 investigation), yielded the following standard r_0 values:

$$r_0(In^+-Br^-) \equiv 266.7\ \text{pm}$$

$$r_0(In^{2+}-Br^-) \equiv 242.0\ \text{pm}$$

$$r_0(In^{3+}-Br^-) \equiv 240.3\ \text{pm}$$

Using these parameters, all empirical valences of In^+ ions fall into the range of 1.00(9), while those of In^{2+} and In^{3+} are 2.00(4) and 3.00(5), respectively. In other words, despite the pronounced differences in coordination polyhedra and effective coordination numbers, the assignment of formal ionic charges is *unambiguously correct*.

It is clear that other bonding influences such as, for example, indium−indium interactions are totally ignored by this concept but they would automatically be included within a quantum mechanical treatment. However, the above parameters should help in the assignment of indium oxidation states within phases yet to be synthesized.

3.2. Quantum Mechanical Computations. A self-consistent study of the binary indium bromides would be a perfect task for a *first principles* technique solving Schrödinger's equation in reciprocal space. Thus, the different ionicities of indium would arise only as the result of the different chemical environments. However, it is the large size of the unit cells of two of the phases which makes this a too challenging project at present time. While In_2Br_3 (80 atoms/unit cell) might still be manageable with great effort, an *ab initio* calculation for In_5Br_7 (192 atoms/unit cell) lies well beyond our computational resources. On the other hand, it would conceptionally be problematic to treat the smaller members (InBr, $InBr_2$, and $InBr_3$) by using an *ab initio* method and the larger members (In_2Br_3 and In_5Br_7) by using a purely empirical one. In this case, other size-dependent error sources would have been introduced and numerical comparisons of overlap populations, charges, etc. would be far from trivial (basis set dependency problems). Therefore, all the five phases were investigated in a self-consistent way but starting from semiempirical Coulomb integrals and using a simplified one-electron Hamiltonian, such as in charge-self-consistent[10] extended Hückel theory.[11] The significance of this approach, however, was tested for the most critical case of InBr by a comparison with one of the most sophisticated *first principles* methods for extended solids (Appendix).

Within the iterative process toward self-consistency, the amount of electron correlation was corrected up to first order "on the fly" by varying all atomic Coulomb integrals dependent on atomic charge and electronic configuration. The charge dependence of the valence orbitals' ionization potentials[12] (VOIPs) was approximated through a quadratic power series. The on-site Hamiltonian matrix elements were first approximated by atomic orbital energies from numerical Hartree−

(9) Brown, I. D.; Altermatt, D. *Acta Crystallogr., Sect. B* **1985**, *41*, 244.
(10) McGlynn, S. P.; Vanquickenborne, L. G.; Kinoshita, M.; Carroll, D. G. *Introduction to Applied Quantum Chemistry*; Holt, Rinehart and Winston: New York, 1972.
(11) Hoffmann, R. *J. Chem. Phys.* **1963**, *39*, 1397.
(12) The sources were average energies of atomic configurations as defined by: Slater, J. C. *Quantum Theory of Atomic Structure*; McGraw-Hill: New York, 1960; Vol. I.

Table 1. Exchange Integral Starting Parameters, Slater Orbital Exponents, and Charge-Iteration Parameters for the Charge-Self-Consistent EH Band Calculations

atom	orbital	H_{ii} (eV)	ζ	A (eV)	B (eV)	C (eV)
In	5s	−10.141	1.934	0.62	8.62	8.17
	5p	−5.368	1.456	0.61	7.14	3.81
	4d[a]	−28.930	3.890	0.34	13.84	15.56
Br	4s	−27.013	2.588	0.00	6.18	24.03
	4p	−12.438	2.131	0.00	10.65	12.35

[a] Note that indium d orbitals were only used for testing purposes in the very first studies on InBr (see text).

Fock calculations,[13] and the Slater-type orbital exponents were based on numerical atomic wave functions (Table 1).[14] The amount of counterintuitive orbital mixing within the minimal basis set was minimized by computing the off-site Hamiltonian matrix elements as defined in the weighted WH formula.[15] The explicit charge iteration parameters (also Table 1) for the In atom were extracted from the work of Munita and Letelier,[16] whereas those of the Br atom[17] were derived from the approximate VOIPs of Basch et al.[18] The configurations used were as follows: s, $d^{n-1}s$; p, $d^{n-1}p$; d, 0.5 ($d^{n-1}s$ + $d^{n-1}p$).

A minimal set of Slater functions for In (5s, 5p) and Br (4s, 4p) was used throughout. The necessity to use or not to use an additional inner 4d orbital on indium was tested from a perturbation theory-like argument. If there would be a 4d influence, it could be expected to be *strongest* in the least oxidized indium ion, namely In^+, since the decrease of screening in the higher charged ions by removal of charge density would move any inner shell such as 4d even closer into the corelike region. Two charge-iterative calculations for the InBr crystal, one including and the other excluding the indium 4d orbitals, converged to cohesive energies (total energies minus atomic eigenvalues) that were equivalent within 1.2%. Moreover, DOS curves above −15 eV were undistinguishable for the naked eye whereas atomic charges differed only by about 0.13%. In short, inner 4d orbitals for the In atom proved to be unnecessary for the discussion of chemical bonding, and they were safely omitted from all subsequent calculations.[19]

4. Computational Results

4.1. General Quantities. Table 2 gives an overview of several energetic findings from the band calculations. There is a strong correlation between the phases' total energies and the molar ratio In:Br, and both variables are linearly correlated throughout the whole range (correlation coefficient = 0.999 97). A similar course for the Fermi energies is not as obvious. The absolute electronic hardnesses[20] reveal the more reduced phases (InBr, In_5Br_7, and In_2Br_3) to be chemically much "softer" than the two others (within Pearson's hard−soft acid−base language) with very similar hardness values around 2.2 eV. In other words, the reduced phases are the most sensitive upon chemical perturbation, in good harmony with the well-known sensitivity of In(I) compounds, especially upon attack of humidity.

Table 2. Total Energies, Fermi Energies, Absolute Hardnesses, and Electrophilic and Nucleophilic Energy Changes of the Five Binary Indium Bromides[a,b]

compound	$\sum\epsilon_i$ (eV)	ϵ_F (eV)	η (eV)	ΔE^{ele} (eV)	ΔE^{nuc} (eV)
InBr	−123.102	−5.115	2.34	−1.72	+6.40
$InBr_{1.4}$ (In_5Br_7)	−165.744	−6.975	2.16	−2.74	+7.06
$InBr_{1.5}$ (In_2Br_3)	−175.682	−6.279	2.29	−2.39	+6.98
$InBr_2$	−230.330	−7.143	3.21	−1.17	+7.60
$InBr_3$	−334.832	−9.440	7.48	+5.43	+9.53

[a] For In_5Br_7 and In_2Br_3, the (extensive) total energies refer to the reduced stoichiometric formulas whereas all other (intensive) quantities are based on the extended formulas (in parentheses). [b] For In_2Br_3 as described by Bärnighausen we arrive at $\sum\epsilon_i$ = −175.786 eV, ϵ_F = −6.253 eV, η = 2.32 eV, ΔE^{ele} = −2.35 eV, and ΔE^{nuc} = +6.99 eV.

Concerning acid−base behavior, the data of the electrophilic energy changes[21] show that In_5Br_7 and In_2Br_3 represent the most electrophilic phases, a result that indicates a possible use of the latter phases as slightly acidic melts or as crystalline host structures for sensitive oxidation states of other metal cations. No clear trend, on the other side, can be deduced from the course of the phases' nucleophilicities.

The small deviations from perfect linear correlation of the total energy−molar ratio function are due to differences in chemical bonding—upon chemical reactions, these numerical deviations (if they were *reliable*) would reflect the fundamental source of nonvanishing reaction enthalpies. Up to now, however, there has not appeared a single thermochemical investigation concerning the latter reaction enthalpies. Our own experimental efforts in the In/Br/M (M = transition metal) systems showed that $InBr_2$ is the favored byproduct of many reactions even at 300−500 °C. Interestingly, even the present calculations would predict that $InBr_2$ is the thermodynamically favored product of a reaction between InBr and $InBr_3$ although it must be emphasized, however, that any such energetic conclusions based on the (approximate variational) charge-iterated EH Hamiltonian may be completely unreliable.

Similarly to the previous bond length−bond strength calculations, the crystal chemical charge assignment is well reproduced. The atomic charges q, calculated via a standard Mulliken partitioning, fall into even narrower ranges of $q(In^+) \approx 0.26(1)$, $q(In^{2+}) \approx 0.467(2)$, $q(In^{3+}) \approx 0.59(2)$, and $q(Br^-) \approx -0.24(3)$, simply because of having taken *all* interatomic influences into account. Since these charges are strongly reduced with respect to the formal valences, covalency seems to play a major role in most of the structures. On the basis of the charge-iterated energy parameters, it is justified to offer averaged exchange integrals for all atoms in different valence states. These values are $H_{5s5s}(In^+) \approx -10.45$ eV, $H_{5p5p}(In^+) \approx -5.71$ eV, $H_{5s5s}(In^{2+}) \approx -12.33$ eV, $H_{5p5p}(In^{2+}) \approx -7.28$ eV, $H_{5s5s}(In^{3+}) \approx -13.50$ eV, $H_{5p5p}(In^{3+}) \approx -8.26$ eV, $H_{4s4s}(Br^-) \approx -22.56$ eV, and $H_{4p4p}(Br^-) \approx -9.81$ eV. They may be used in subsequent semiempirical calculations on even more complex compounds, having unit cells far too large to be treated by a self-consistent procedure.

In the following, we will focus on the chemical bonding, with a special emphasis on the univalent indium cations. Again, the crystal−chemical labeling is in accord with the original structure communications and the supplementary material.

4.2. Chemical Bonding in $InBr_3$. The density-of-states (DOS) curve for $InBr_3$ (Figure 9) is the result of highly ionic

(13) Desclaux, J. P. *At. Data Nucl. Data Tables* **1973**, *12*, 311.
(14) Pyykkö, P.; Lohr, L. L., Jr. *Inorg. Chem.* **1981**, *20*, 1950.
(15) Ammeter, J. H.; Bürgi, H.-B.; Thibeault, J. C.; Hoffmann, R. *J. Am. Chem. Soc.* **1978**, *100*, 3686.
(16) Munita, R.; Letelier, J. R. *Theor. Chim. Acta (Berlin)* **1981**, *58*, 167.
(17) They are very similar to those formerly used for calculations on rare earth metal trihalide molecules. See: Myers, C. E.; Norman, L. J., II; Loew, L. M. *Inorg. Chem.* **1978**, *17*, 1581.
(18) Basch, H.; Viste, A.; Gray, H. B. *Theor. Chim. Acta (Berlin)* **1965**, *3*, 458.
(19) The computations on InBr (8 atoms, 40 valence electrons, 72 *k* points), In_2Br_3 (≡$InBr_{1.5}$; 80 atoms, 432 valence electrons, 8 *k* points), $InBr_2$ (24 atoms, 136 valence electrons, 36 *k* points), and $InBr_3$ (16 atoms, 96 valence electrons, 72 *k* points) were carried out on a DECstation 5000/133 while the computation on In_5Br_7 (≡$InBr_{1.4}$; 192 atoms, 1024 valence electrons, 16 *k* points) was performed on a CONVEX 3830. Self-consistency was reached after 13 (InBr), 19/19 (In_2Br_3 within the centric/acentric description), 22 ($InBr_2$), 22 ($InBr_3$), and 19 cycles (In_5Br_7).
(20) Parr, R. G.; Pearson, R. G. *J. Am. Chem. Soc.* **1983**, *105*, 7512.
(21) Both theoretical and experimental concepts for acid−base behavior of solids are beginning to emerge. See: Dronskowski, R. *J. Am. Chem. Soc.* **1992**, *114*, 7230. O'Donnell, T. A. *Super-Acids and Acidic Melts as Inorganic Chemical Reaction Media*; VCH Publishers: Weinheim, New York, Cambridge, 1993.

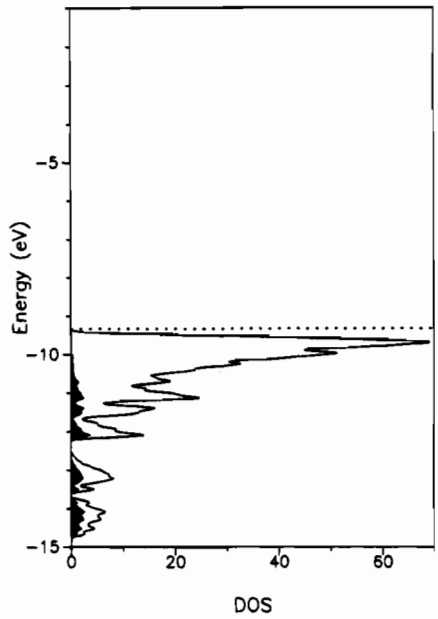

Figure 9. Density-of-states (DOS) of $InBr_3$, with local DOS of In^{3+} emphasized in black.

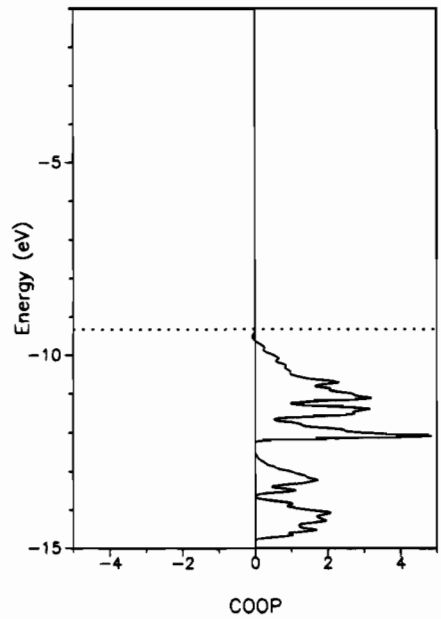

Figure 10. Crystal-orbital-overlap-population (COOP) of the $In^{3+}-Br^-$ bonding ($d \leq 300$ pm; 24 bonds/cell) within $InBr_3$.

bonding in this simplest phase. Regardless of the very low-lying Br s-centered levels around −24 eV (not visible here but always present in all of the compounds), bonding between In s/p and the Br p orbitals takes place roughly between −15 and −9 eV. A detailed analysis shows that indium s participation is energetically restricted to lie below −12.3 eV while indium p orbitals mix in above that energy threshold. There is a huge band gap of more than 14 eV, the virtual bands not being appreciable within the chosen energy window.

The build-up of In−Br bonding (Figure 10) is seen in the shape of the COOP curve paralleling the course of the preceding indium DOS, with practically no antibonding interactions visible. More quantitatively, the integrated crystal orbital overlap population (ICOOP) for this formal $In^{3+}-Br^-$ interaction (six bonds ranging from 265 to 268 pm) has a value of +0.441.[22]

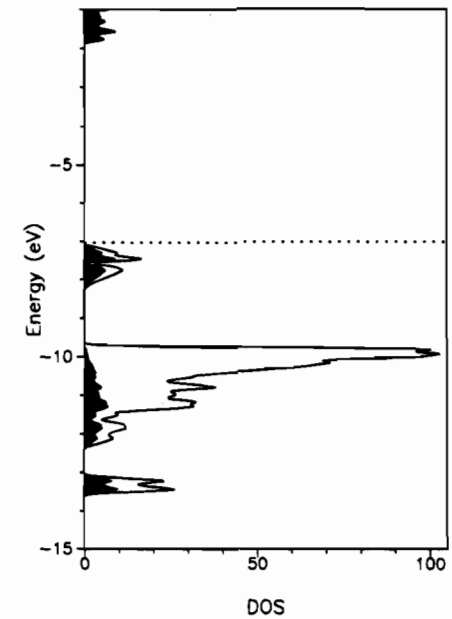

Figure 11. Density-of-states (DOS) of $InBr_2$, with local DOS of In^+ and In^{3+} emphasized in black.

The In^{3+} ion carries the highest charge of all coming indium ions, namely +0.610. Consequently, only some slightly repulsive $In^{3+}-In^{3+}$ interactions (ICOOP = −0.084) exist within the structure, in perfect harmony with the simplest (electrostatic) interpretation. In short, quantum mechanics shows that a purely electrostatic description of the bonding within $InBr_3$ is almost satisfactorily accurate.

4.3. Chemical Bonding in $InBr_2$. By use of Figure 11, showing the global and local (indium) DOS of $InBr_2$, one may easily distinguish between In^+ and In^{3+}. Both univalent and trivalent ions mix into the medium energy range between −9.5 and −12.5 eV, the In^{3+} ion having a little higher contribution here. The DOS spike around −13.3 eV, however, is almost completely In^{3+} in character. Its splitting for tetrahedral In^{3+} coordination is comparatively smaller than the octahedral splitting within $InBr_3$, in accord with ligand field−theoretical arguments. The presence of an In^+ ion is clearly apparent from the frontier DOS around −7.5 eV, touching the Fermi level, which lies about 2 eV higher than in the case of $InBr_3$. And there are virtual In^+-centered bands, separated by a band gap of more than 5 eV.

Concerning the bonding of In^{3+} and In^+ to Br^-, one only finds bonding $In^{3+}-Br^-$ interactions (four bonds between 250 and 251 pm), roughly between −10 and −14 eV, with an average ICOOP of +0.646 (COOP figure omitted for brevity). By contrast, In^+-Br^- bonding (Figure 12) is characterized both by bonding levels between −10 and −14 eV *and* by a surprisingly strong *antibonding* interaction very close to the Fermi level. As an anticipation of things to come, all formal In^+-Br^- interactions can thus be characterized as having these strongly antibonding frontier bands in common. Consequently, the bonding (eight bonds between 342 and 349 pm) is significantly *weak*. Even taking into account the larger In^+-Br^- distances, the *much* smaller ICOOP value of +0.078 is astonishing because it is so little.

One can clarify the nature of this antibonding In^+-Br^- interaction from an MO model calculation[23] of a perfectly cubic $InBr_8^{7-}$ unit that has constant metal−nonmetal distances of 345 pm (similar to the polyhedron seen in Figure 1). In the end,

(22) Here and in the following, ICOOPs are expressed as averaged values over all nearest-neighbor interactions.

(23) Program CACAO by: Mealli, C.; Proserpio, D. M. *J. Chem. Educ.* **1990**, *67*, 399.

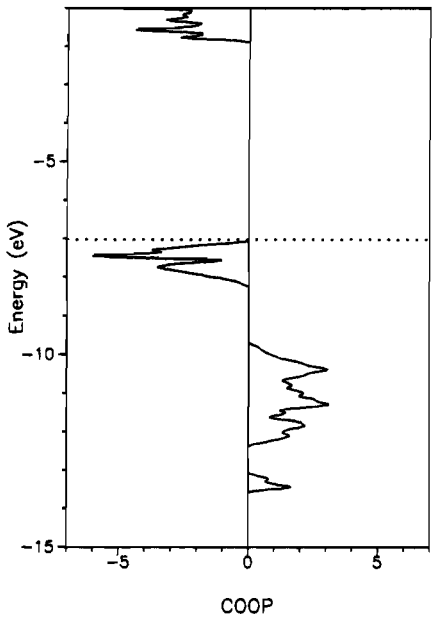

Figure 12. Crystal-orbital-overlap-population (COOP) of the In^+-Br^- bonding ($d \leq 400$ pm; 32 bonds/cell) within $InBr_2$.

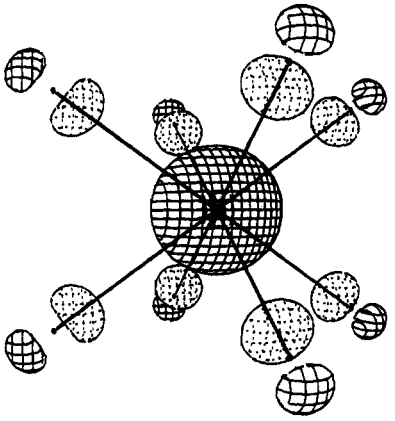

Figure 13. HOMO wave function of a cubic $InBr_8^{7-}$ species, using a 345 pm long In^+-Br^- distance. The surface value of the molecular orbital is 0.075. For clarity, atomic orbital contributions have been contracted by a factor of 1.5.

one finds a strongly antibonding HOMO wave function at roughly −7.4 eV, depicted in Figure 13. This wave function has a_{1g} symmetry and it arises from the out-of-phase combination between the indium 5s orbital and the corresponding p hybrids located on the eight cube bromine ions, pointing inside toward In^+ along the cube's diagonal. Somewhat simplified, this indium-centered HOMO wave function incorporates the two additional electrons of In^+ compared to In^{3+}. Thus, internal reduction of indium from the trivalent to the monovalent state has to be paid by weakened In^+-Br^- bonding. Equally analogous to the COOP spike of the solid, the antibonding HOMO lies more than 2 eV higher than the lower bonding levels, indicating an (energetically) localized orbital within the delocalized crystal orbitals. Upon lowering of symmetry and because of second nearest neighbor interactions in the solid, however, some broadening from mixing into this level occurs (Figure 12).

At last, any *directed* p-like "lone-pair" contribution of In^+ can be rejected by comparing Figures 11 and 12. There is no single DOS spike for In^+ that does not show up equally as a bonding or antibonding effect—by definition, however, a "lone-pair" must be (almost) *nonbonding*. Still in harmony with

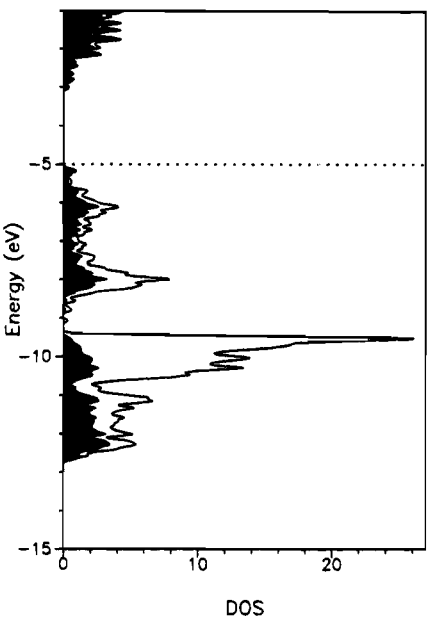

Figure 14. Density-of-states (DOS) of InBr, with local DOS of In^+ emphasized in black.

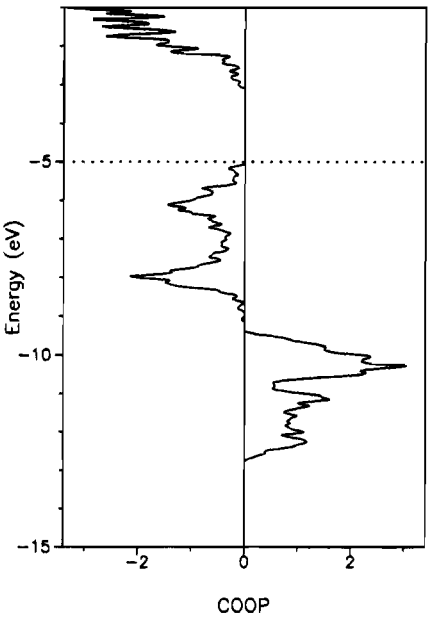

Figure 15. Crystal-orbital-overlap-population (COOP) of the In^+-Br^- bonding ($d \leq 400$ pm; 28 bonds/cell) within InBr.

electrostatics, the In^+-In^{3+} interaction (ICOOP = −0.033) is slightly repulsive.

4.4. Chemical Bonding in InBr. The DOS curve of InBr (Figure 14) is characterized by the large contribution of indium levels close to the frontier bands. Whereas the total In participation is apparent from a wide energy block between −5 and −13 eV, with a tentative inner gap just below −9 eV, another decomposition shows that there is a negligible indium p contribution, restricted to an energy window between −9.5 and −10.5 eV. In this most reduced phase, a small band gap of less than 2 eV separates indium p-dominated virtual bands from the occupied band regions.

Figure 15 gives an overview of the averaged In^+-Br^- interactions of the seven nearest bonds (mean bond length 342 pm). As in the case of monovalent In^+ inside $InBr_2$, there is again visible a region of strong antibonding nature close to the Fermi level, almost completely due to In s and Br p wave functions. A plot of the corresponding molecular HOMO can

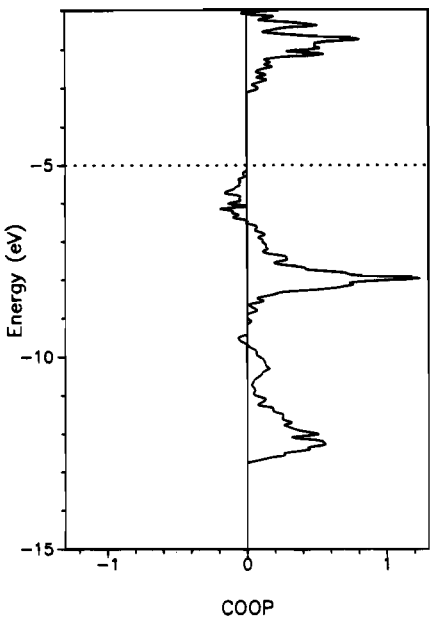

Figure 16. Crystal-orbital-overlap-population (COOP) of the In^+-In^+ interactions (d ≤ 380 pm; 4 bonds/cell) within InBr.

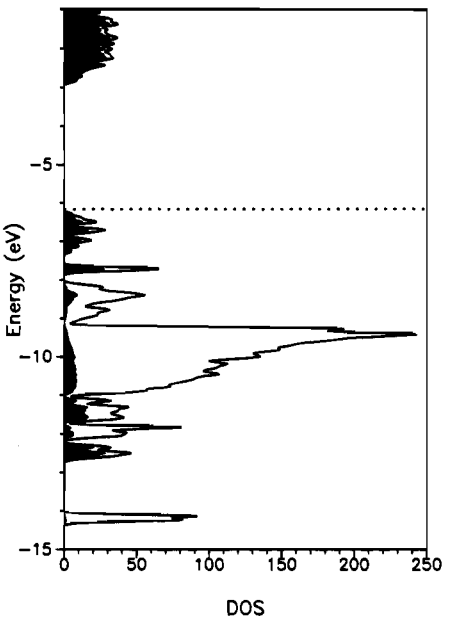

Figure 17. Density-of-states (DOS) of In_2Br_3 (centric description), with local DOS of monovalent indium ions (In(4–6)) emphasized in black.

be constructed *by hand* from Figure 13 upon removing one ligand and rearranging the remaining bromine ions appropriately. The small In p contribution is located in the *bonding* spike around −10 eV, and the average ICOOP (+0.084) is slightly higher than the one for In^+ inside $InBr_2$. Most significantly, there are *bonding* interactions (ICOOP = +0.293) between the In^+ ions (355 pm distance) apparent (Figure 16). A numerical energy partitioning scheme shows that, on the basis of the one-electron approximation applied here, about 35% of the total off-site (bonding) energies can be traced back to this bonding metal–metal interaction. Note that the latter is essentially nondirectional since the p contribution to it (at around −10 eV) is negligible in size—in other words, even the In^+-In^+ bonding is by no means due to a directed orbital.

Both In^+-In^+ and In^+-Br^- interactions inside InBr can be characterized from those striking antibonding effects at the frontier bands, a clear sign that InBr must be very easily oxidizable. Indeed, experimental experience shows that InBr is an eager reducing agent and it decomposes when brought into contact with almost any oxidizing media such as, for example, water, promoting the disproportionation into $InBr_3$ and metallic In.

4.5. Chemical Bonding in In_2Br_3. This section is based on the centric picture of the In_2Br_3 crystal structure, the comparison with the acentric description following in section 4.5.1. The DOS curve of In_2Br_3 is given in Figure 17, the local contributions of the monovalent In^+ ions emphasized in black. In^+ ions contribute to a broad region, starting above −13 eV and going up to the Fermi energy. The virtual bands, more than 3 eV apart, are also almost completely In^+ (p) in character. The divalent In^{2+} ions, on the other side, mix into a slightly smaller energy range between −8 and −13 eV, and there is a very small spike just below −14 eV dominated by In^{2+}.

Among the monovalent indium ions, however, another distinction is possible. One In^+ ion (In(4); see Figure 3 for coordination) is responsible for the sharp ("lone-pair"?) DOS spike at −7.7 eV, and it does not contribute to any higher occupied bands. This is done by the two other monovalent In^+ ions (In(5) and In(6); see Figures 4 and 5), both having almost the same DOS. In other words, the before-mentioned crystal–chemical difference between 8-fold and 9-fold bromine coordination (In(5) *vs* In(6)) does *not* emerge in the electronic structure but is an artifact of crystal–chemical notion.

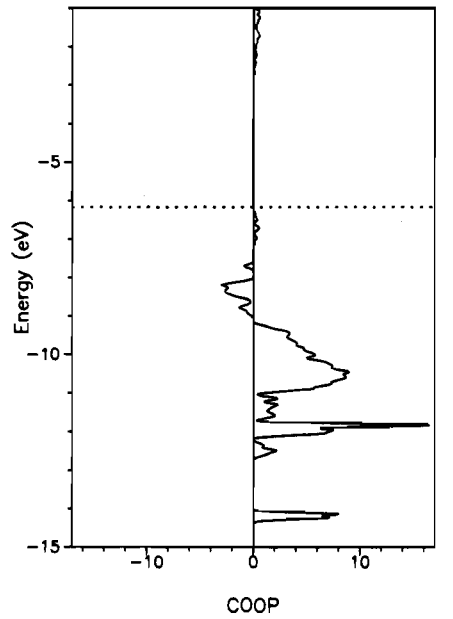

Figure 18. Crystal-orbital-overlap-population (COOP) of the $In^{2+}-Br^-$ bonding (In(1–3) ions; d ≤ 300 pm; 48 bonds/cell) within In_2Br_3.

To find the origin of the sharp DOS spikes of both the divalent ions and the monovalent In(4) ion, a little detective work is needed. Figure 18 represents the bonding between divalent In^{2+} ions and surrounding Br^- ions inside the anionic unit (Figure 6). With the exception of a small antibonding tip around −8.5 eV, one finds strong $In^{2+}-Br^-$ bonding within the In-augmented tetrahedron (ICOOP = +0.567). The DOS spike below −14 eV, however, is still easier to recognize in the corresponding COOP of the $In^{2+}-In^{2+}$ interaction, depicted in Figure 19. This is the deep-lying $In^{2+}-In^{2+}$ *single bond*, well-separated in energy and space from the remaining structure; its averaged ICOOP value is very large (+0.900) for a bond distance of 270 pm. Another MO model calculation[23] on such an $In_2Br_6^{2-}$ unit leads to the same conclusion: The indium 5s contribution to the strongly localized MO around −14 eV (Figure 20) is twice as large as the 5p contribution along the internuclear direction,

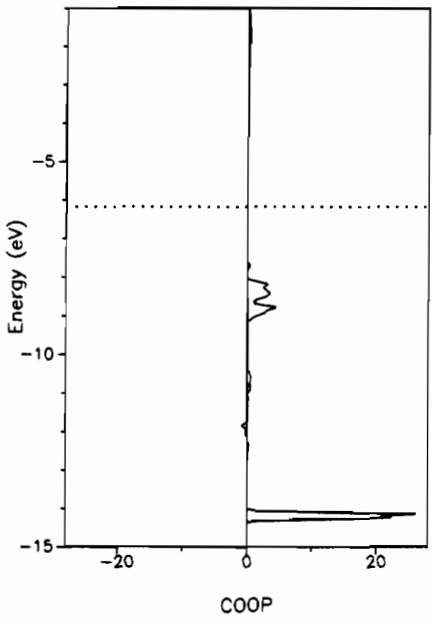

Figure 19. Crystal-orbital-overlap-population (COOP) of the $In^{2+}-In^{2+}$ bonding (In(1−3) ions; d ≤ 300 pm; 8 bonds/cell) within In_2Br_3.

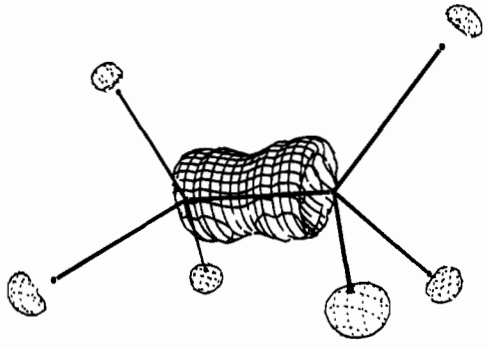

Figure 20. Deep-lying (−14 eV) molecular wave function of the $In_2Br_6^{2-}$ dimeric unit inside In_2Br_3, the main contributor to the $In^{2+}-In^{2+}$ single bond. The surface value of the molecular orbital is 0.075. For clarity, atomic orbital contributions have been contracted by a factor of 1.5.

the perpendicular (π-like) p's mixing in 20 times weaker than 5s—a true single bond.

Concerning the monovalent In(4) ion's bonds to Br^- neighbors, Figure 21 shows that the DOS spike (−7.7 eV) *cannot* be attributed to a directed "lone-pair" wave function. On the contrary, it originates from a strongly *antibonding* interaction which has already been visualized in Figure 13, namely the out-of-phase combination between indium 5s and bromine p orbitals. Because of the In(4) coordination polyhedron's high symmetry (monocapped cube in Figure 3), virtually no level broadening has occurred in the crystal. In total, In(4)−Br bonding (ICOOP = +0.073, nine bonds from 349 to 438 pm) is very similar to that of monovalent In^+ within $InBr_2$.

A slightly different situation is found for the bonding of In(5) and In(6), perceptible from Figure 22. This COOP curve resembles the one of In^+-Br^- bonding inside InBr, with a broad antibonding region close to the Fermi level. In^+-Br^- bonding of In(5) and In(6) is slightly weaker (ICOOP = +0.065 and +0.056) at these sites. It is logical that these should be the non-fully occupied sites provided that In_2Br_3 is described by use of a centric unit cell.

4.5.1. Centric or Acentric In_2Br_3? As has been explained in section 2, there are two different descriptions of the In_2Br_3 crystal structure available. Upon taking an unbiased look at

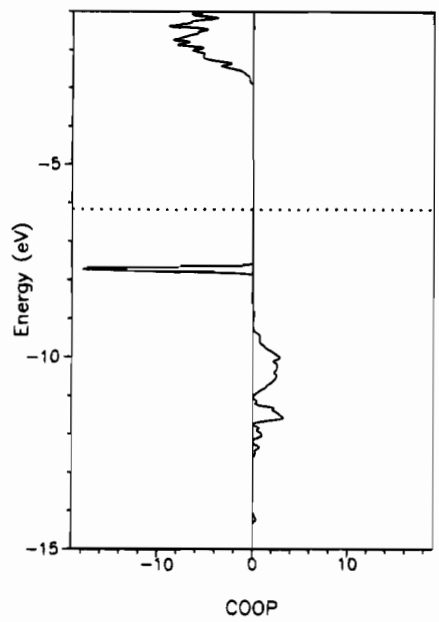

Figure 21. Crystal-orbital-overlap-population (COOP) of the In^+-Br^- bonding (In(4) ion; d ≤ 450 pm; 36 bonds/cell) within In_2Br_3.

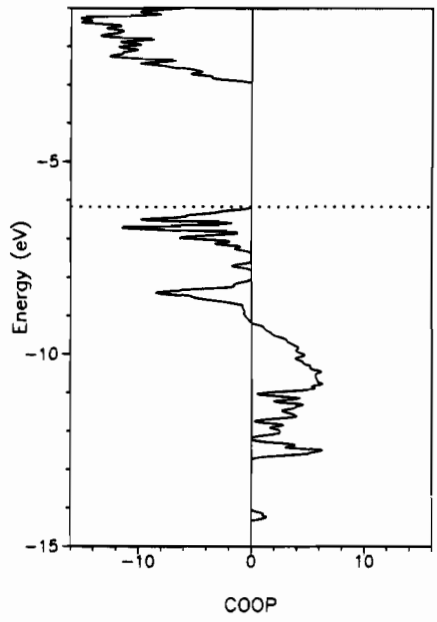

Figure 22. Crystal-orbital-overlap-population (COOP) of the In^+-Br^- bonding (In(5) and In(6) ions; d ≤ 450 pm; 102 bonds/cell) within In_2Br_3.

the X-ray data, the centric description seems to be clearly inferior compared to the acentric description[24] although it is almost impossible to estimate the different intrinsic crystal qualities of the two specimens that were under investigation. The main dissent between the two alternatives lies only in the characterization of two 75% occupied monovalent indium ions (labeled In(5) and In(6) in the centric model; see Figures 4 and 5). In the case of a centrosymmetric space group, each of two neighboring polyhedra (Figure 23) are 75% occupied with those univalent indiums. Consequently, there is a finite probability for a short (317 pm) In^+-In^+ bond since both polyhedra may be filled with In^+ *at the same time*. If described by a

(24) *Centric* description: 3497 reflections of which 1036 with $|F_o| > 2\sigma(F_o)$; overdetermination (number of reflections/number of variables) about 10; $R_w = 0.069$. *Acentric* description: 2532 reflections (no standard deviation limit); overdetermination greater than 13; $R_w = 0.024$.

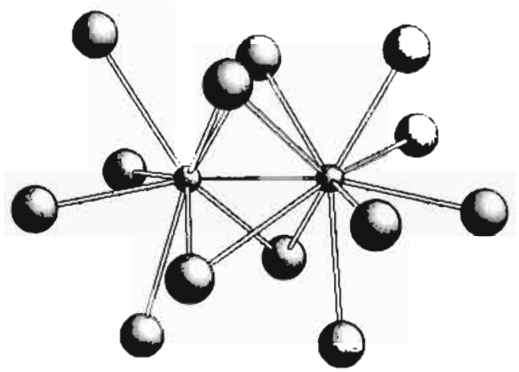

Figure 23. Possible short contact (317 pm) between monovalent indium ions within a centric description of the In_2Br_3 structure. The view direction is close to [010]. For the centric case (In(5), left, and In(6), right, show 75% site occupation) there is a finite chance for such an In^+-In^+ contact. No contact, however, is found for the acentric case where either the left or the right polyhedron is occupied.

noncentrosymmetric space group, on the contrary, the neighboring polyhedra are *alternately* occupied throughout the structure. *Thus, the choice of the space group decides between the presence (centric space group) or absence (acentric space group) of an In^+-In^+ partial bond.*[25] From the most primitive, electrostatic point of view, the centric description is unfavorable because of In^+-In^+ *repulsion*; however, the need for the acentric description only showed up from the violation of zonal extinction rules.[3]

Without questioning the more accurate acentric structure determination of In_2Br_3, skillfully extracted from an X-ray study on polysynthetic inversion twins, how much truth could there be within a centric picture? Is it possible that one can still find partially bonded In^+-In^+ pairs, probably existing in certain "centric defects" inside an otherwise acentric crystalline material?[26] The two alternatives in structural description were compared by use of charge-iterated electronic structure calculations. Statistical occupancy of In^+ ions was approximated by filling only $^3/_4$ (when encountering 75 and 79% occupancy) and $^1/_4$ (at 21% occupancy) of the equivalent sites. The centric scenario, incorporating above-mentioned In^+-In^+ partial bond, would be favored by a strong (ICOOP = +0.587) covalent interaction (Figure 24), weaker than the $In^{2+}-In^{2+}$ single bond within In_2Br_3 but stronger than the In^+-In^+ contact within InBr. The most prominent bonding peak lies at −8.5 eV, mirrored as an *antibonding* interaction in the In^+-Br^- COOP plot (refer to Figure 22). Thus, the two interactions (In^+-In^+ and In^+-Br^-) are *competitive*, their main energy difference converging to a nonzero value only if centric and acentric alternatives should be truly different.[27]

Table 2 reveals that the total energy of In_2Br_3 is lower (0.06%) in the *acentric* than in the centric description by roughly 20 kJ/mol of In_2Br_3 or 320 kJ/unit cell (16 formula units). Also, the absolute hardness increases by about 1% for the *acentric* structure. Since the two structure determinations differ in temperature by 80 °C during data collection, another energy

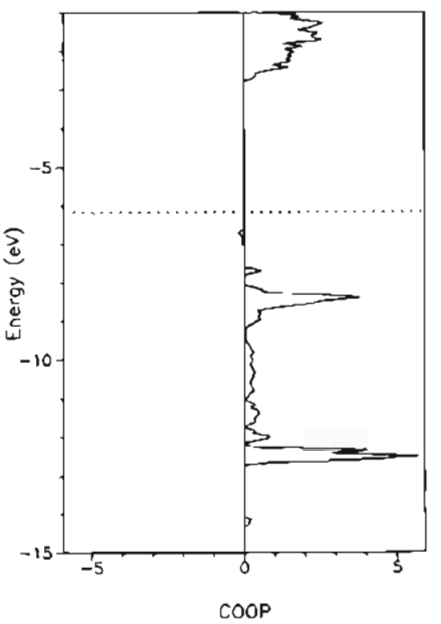

Figure 24. Crystal-orbital-overlap-population (COOP) of the In^+-In^+ bonding (partially occupied In(5) and In(6) ions; $d \leq 350$ pm; 6 bonds/cell) within In_2Br_3 (centric description).

correction has to account for the influence of the differing lattice parameters.[28] Thus, the intrinsic energy difference only due to the temperature gradient lies at about 10 kJ/mol, leaving the remaining 10 kJ/mol (160 kJ/cell) to result from the real difference in structural description (centric or acentric alternative; In^+-In^+ partial bonds allowed or forbidden).

This energy difference of 160 kJ/cell, measuring the competition between In^+-In^+ and In^+-Br^- bonding seems to be quite reliable, even considering the limited accuracy of the method and the model used—no typical EH error source (bending angles, stretching bonds, etc.) is present. Since this amount of energy is the result of attractive In^+-In^+ interactions (statistically allowed six times within one centrosymmetric unit cell)—by that considerably weakening In^+-Br^- bonding—nature would have to pay roughly $160/6 \approx 27$ kJ to form a single such In^+-In^+ partial bond (317 pm). Finally assuming Maxwell–Boltzmann statistics for the generation of (i) In^+-In^+ pairs (centric case) and (ii) alternate occurrence of In^+ in neighboring polyhedra (acentric case), the ratio of presence between both alternatives can be expected to lie around $1:(6 \times 10^{14})$ at room temperature. Thus, although truly favoring the acentric structure it would still allow the existence of about 10^{14} In^--In^+ partial bonds (centric defects) inside an otherwise acentric single crystal which is 1 mm^3 in volume—thus, even a temperature-dependent equilibrium between centric and acentric macroscopic domains within crystalline In_2Br_3 might well be possible.

4.6. Chemical Bonding in In_5Br_7. Roughly speaking, the structure of In_5Br_7 is just an enlarged variant of the In_2Br_3 type, yet the bonding is easier to understand. Figure 25 provides the total DOS of In_5Br_7 and the corresponding local DOS of the monovalent indium ions. There are wide In^+ contributions starting at −12.5 and going up to the Fermi level (close to −7 eV), and also the virtual levels, about 4 eV apart, are almost completely dominated by In^+ (p). To our surprise, the simple

(25) Technically speaking, any In^+-In^+ bond is excluded while (i) using an acentric space group ($P2_12_12_1$) and (ii) splitting "centric In(5)" into the "acentric In(6b)/In(7)" pair and "centric In(6)" into the "acentric In(5)/In(6a)" pair, provided that (iii) In(6a) and In(6b) are alternately occupied (79 and 21%).

(26) Due to statistical appearance, these defects would probably be invisible for X-rays although eventually detectable by use of nuclear magnetic resonance techniques.

(27) Provided such a bonding, the two In^+ ions could be regarded as emerging In^{2+} ions, and their significantly enlarged atomic charges (+0.275 for In(5) and +0.299 for In(6)) would substantiate that interpretation.

(28) The heat capacities for InBr and $InBr_3$ were tabulated by: Knacke, O.; Kubaschewski, O.; Hesselmann, K. *Thermochemical Properties of Inorganic Substances*; Springer: Berlin, Heidelberg, New York, London, Paris, Tokyo, Hong Kong, Barcelona, Budapest; Verlag Stahleisen m.b.H.: Düsseldorf, 1991. One may then interpolate an average heat capacity for In_2Br_3 (about 123 J/K mol) within a temperature range between −60 and 20 °C.

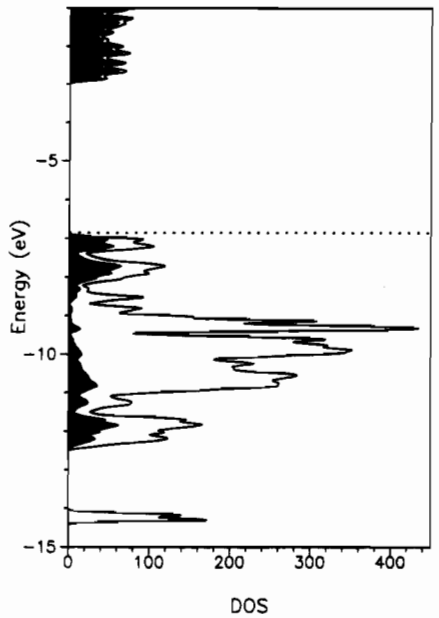

Figure 25. Density-of-states (DOS) of In_5Br_7, with local DOS of monovalent indium ions (In(1−7)) emphasized in black.

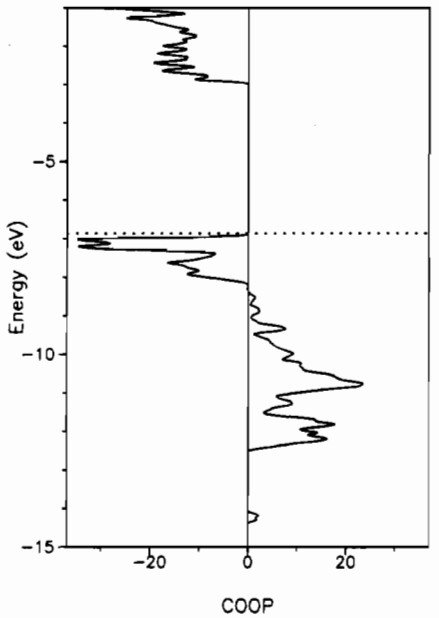

Figure 26. Crystal-orbital-overlap-population (COOP) of the In^+-Br^- bonding (9-fold coordinated In(1−4) ions; d ≤ 450 pm; 288 bonds/cell) within In_5Br_7.

grouping into nine-coordinated (In(1−4), Figure 7) and ten-coordinated In^+ ions (In(5−7), Figure 8) actually proves to be true. Because of their average In^+-Br^- distances being about 8 pm shorter in magnitude, the dispersion of the local DOS of the nine-coordinated In^+ ions is nearly one electronvolt larger than the one of the ten-coordinated In^+ ions.[29]

The interaction of the divalent In^{2+} ions with the host lattice, on the other side, is energetically restricted to an energy window between −8 and −12.5 eV. There is also an additional DOS spike just below −14 eV, very much resembling the one visible for the $In^{2+}-In^{2+}$ dimer inside In_2Br_3.

Figures 26 and 27 give the COOP plots of the In^+-Br^- bonds, both for 9-fold and 10-fold coordination of In^+. The

(29) Consequently, the DOS of Figure 25 resembles the one of two superimposed s lattices that have a slightly different translational vector or interaction range.

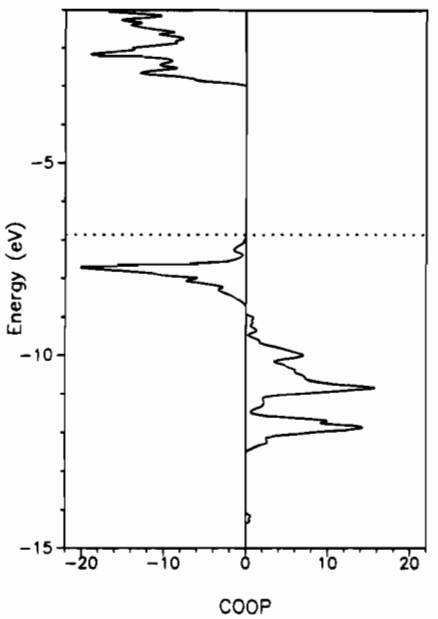

Figure 27. Crystal-orbital-overlap-population (COOP) of the In^+-Br^- bonding (10-fold coordinated In(5−7) ions; d ≤ 450 pm; 160 bonds/cell) within In_5Br_7.

overlap contribution of In^+ is mostly s in character, with a very small p participation around −10.5 eV. As was indicated before in the DOS discussion, the bonding of the "9-fold couples" is more dispersed than the bonding of the "10-fold couples", the peak of the antibonding levels touching the Fermi level only in the first case. This implies an easier access to the In(1−4) sites upon oxidation which may be of value in the course of performing soft chemical studies on In_5Br_7. However, numerical data for the In^+-Br^- interactions result in an average ICOOP of +0.071,[30] in very good agreement with the In^+-Br^- bonding of the other phases. It is clear that In^+-Br^- bonding follows the same rule in all cases: Bromine p hybrids, out-of-phase with respect to an indium 5s orbital, may "float" on a sphere around In^+ without thus changing the antibonding nature of this interaction and the overall energetics, provided that Br^--Br^- repulsion has been sufficiently taken care of. Indium p participation, however, does not play a significant role.

For the case of the divalent In^{2+} ions within the $In_2Br_6^{2-}$ units, the $In^{2+}-Br^-$ COOP (omitted for brevity) reflects full equivalency with the situation inside In_2Br_3 (Figure 18), showing that the anionic units are electronically uninfluenced by the different host structures. The strength of the $In^{2+}-Br^-$ bonding (ICOOP = +0.561) is only 1% smaller in magnitude than it is in In_2Br_3. Also, the COOP of the $In^{2+}-In^{2+}$ single bond matches the one of In_2Br_3 (Figure 19) and the single bond (ICOOP = +0.888) is also only about 1% weaker than before.

5. In^+-Br^-: A Second-Order Jahn−Teller Effect?

It is typical for all monovalent indium cations inside bromine polyhedra that they show an unexpected small degree of s−p mixing. As an exemplary consequence, the essential idea of their chemical bonding can be readily visualized from Figure 13: For a cubic $InBr_8^{7-}$ unit, there is a HOMO wave function of mostly indium 5s character, separated from a triply degenerate LUMO where the indium 5p atomic orbitals mix in. It is due to point group symmetry reasons that there can be no s−p mixing here. However, how strong would the mixing become upon In^+ displacement?

(30) In detail, the values are +0.069 for In(1) and In(2), +0.075 for In(3) and In(4), +0.071 for In(5), +0.069 for In(6), and +0.070 for In(7).

This interesting possibility, spotted by a perceptive reviewer, could then be understood to originate from a second-order Jahn–Teller effect; a small energy gap between HOMO and LUMO would allow an intermixing between them because of their susceptibility to a (possibly spontaneous) structural distortion. Upon computation, one might expect to detect such phenomenon most easily in the more symmetrical In^+/Br^- polyhedra (see Figures 1 and 3) compared to the other ones (see Figures 2, 4, 5, 7, and 8) where the local symmetry is quite low.

Corresponding model calculations on originally cubic $InBr_8^{7-}$ units that had been subject to small shifts of the In^+ ion along the 2-, 3-, and 4-fold axes gave a two-sided result. For a constant step size of 1 pm and dislocations up to 30 pm, there is *no* lowering or relative minimum found both for the total energy and for the energy of the HOMO so that a definite second-order Jahn–Teller effect *cannot* be confirmed. On the other hand, the differences for the energy hypersurface upon shifting the indium cation away from its origin are extraordinarily small: Only about 2 kJ, for example, is required for a 20 pm shift of In^+ along any of the three main symmetry axes. Considering the limited accuracy of the present wave mechanical method and its parametrization (for example the somewhat too small underlying 5s–5p energy separation; see Appendix), the significance of the here found energy value is certainly questionable. However, such a tiny energy difference, reflecting a very soft crystal potential for In^+, would perfectly explain why *all* related X-ray crystallographic studies show significantly enlarged In^+ displacement parameters even at full site occupancy. Indeed, In^+ may be subject to "trembling motions" around its equilibrium site because the activation barriers are so very small.

6. Summary

The complexity of the crystal structures of the binary indium bromides is mainly due to the local electronic structure of the monovalent indium ions: Their coordination polyhedra's strong irregularities reflect the impact of the almost doubly filled indium 5s orbital on the chemical bonding—since the latter has no directional tendency, any bromine polyhedron giving sufficient space for In^+, aside from repelling $Br^- - Br^-$ interactions, is *equally appropriate* and leads to *similar* bonding energies. A stereaoactive influence of a *directed* electron "lone-pair" orbital *cannot* be detected.

All $In^+ - Br^-$ bonds are characterized by showing strong *antibonding* effects close to the Fermi energy, resulting from an out-of-phase combination between 4p hybrids of coordinating bromine ions and a central indium 5s atomic orbital. This unusual and intrinsically destabilizing effect is the reason for the high chemical sensitivity and small electronic hardness of reduced indium bromides containing In^+. The latter ion exhibits an electrophilic tendency (striving for being neutral) such that In_2Br_3 and In_5Br_7 may be expected to serve usefully as slightly acidic melts or as host structures for the stabilization of sensitive oxidation states of guest cations.

(31) QCPE program EHMACC by M.-H. Whangbo, M. Evain, T. Hughbanks, M. Kertesz, S. Wijeyesekera, C. Wilker, C. Zheng, and R. Hoffmann.
(32) Andersen, O. K. *Phys. Rev. B* **1975**, *12*, 3060.
(33) Andersen, O. K.; Jepsen, O.; Glötzel, D. In *Highlights of Condensed-Matter Theory*; Bassani, F., et al., Eds.; North-Holland: New York, 1985.
(34) Skriver, H. L. *The LMTO Method*; Springer: Berlin, Heidelberg, New York, 1984.
(35) Andersen, O. K.; Jepsen, O.; Sob, M. In *Electronic Band Structure and its Applications*; Yussouff, M., Ed.; Springer: Berlin, Heidelberg, New York, 1986.
(36) Korringa, J. *Physica* **1947**, *13*, 392.
(37) Kohn, W.; Rostoker, N. *Phys. Rev.* **1954**, *94*, 1111.

Table 3. Semiempirical Charge-Iterated Exchange Integrals H_{ii} and Self-Consistent *ab Initio* Band Centers C for InBr

atom	orbital	H_{ii} (eV)	C (eV)
In	5s	−10.399	−9.559
	5p	−5.662	−0.490
	5d		+24.314
Br	4s	−22.461	−19.306
	4p	−9.646	−6.734
	4d		+13.616

Acknowledgment. It is a pleasure to thank Prof. Dr. Arndt Simon (Stuttgart) for his steady and generous support. The author would also like to thank Prof. Dr. Clifford E. Myers (Binghamton, NY) as well as Dr. Pere Alemany (Barcelona, Spain) for their expert help in generating reliable charge-iteration parameters for the Br atom. Additional thanks are directed to Prof. Dr. Robert E. McCarley for providing valuable suggestions on this paper while being on a sabbatical visit at the Max-Planck-Institute in late 1993. A copy of the original EHMACC program[31] was supplied by Prof. Dr. Reinhard Nesper (Zürich, Switzerland) whereas the additional charge-iteration subroutine was built in by one of his co-workers, Dr. Ulrich Häussermann. The author is indebted to both of them. Further financial support by the Fonds der Chemischen Industrie (Frankfurt) is gratefully acknowledged.

Appendix: First Principles Calculations on InBr

The relative energy ordering of the indium orbitals is of critical importance for the validity of the semiempirical band structure calculations. In particular, the (surprisingly small) degree of s–p mixing observed, leading to the (unexpected) strongly antibonding $In^+ - Br^-$ interactions below the Fermi level, may need further theoretical verification. In order to test the significance of the semiempirical Hamiltonian and the charge-iterative procedure, electronic structure calculations of *ab initio* quality were performed for the (smallest) case of InBr using LMTO (Linear Muffin-Tin Orbital) theory,[32-35] a fast linearized form of the KKR method.[36,37] It accounts for the potential from all the electrons and its almost minimal, unfixed basis sets adjust dynamically to the respective potentials. In the interstitial regions with flat potentials, the wave functions of the valence electrons are expanded into Hankel envelope functions whereas in the corelike regions one seeks numerical solutions of the radial Schrödinger equation.

The electronic energy of InBr was computed with the help of density-functional theory, replacing the many-particle problem by the self-consistent solution of the Kohn–Sham equations,[38,39] taking the von Barth and Hedin parametrization[40] and using a non-spin-polarized scalar relativistic Hamiltonian. The integration in k space was performed with the help of an improved[41] tetrahedron method[42] such that with 138 inequivalent k points and 1450 different tetrahedra k convergence was better than 1 meV.[43] A minimal basis set of short-range atom-centered TB-LMTO's was used,[44] that is, one s, three p, and five d orbitals on In and Br atoms plus a large number of polarization functions in the interstitial regions (atomic-spheres approximation (ASA) "empty spheres" technique). Indium and bromine d orbitals were included using a downfolding technique. Starting from atomic Hartree potentials, the structure was

(38) Hohenberg, P.; Kohn, W. *Phys. Rev. B* **1964**, *136*, 864.
(39) Kohn, W.; Sham, L. J. *Phys. Rev. A* **1965**, *140*, 1133.
(40) von Barth, U.; Hedin, L. *J. Phys. C* **1972**, *5*, 1629.
(41) Blöchl, P. Ph.D. Thesis, Universität Stuttgart, 1989.
(42) Jepsen, O.; Andersen, O. K. *Solid State Commun.* **1971**, *9*, 1763.
(43) This corresponds to a 50% smaller primitive monoclinic setting of the orthorhombic C-centered crystallographic unit cell.
(44) Andersen, O. K.; Jepsen, O. *Phys. Rev. Lett.* **1984**, *53*, 2571.

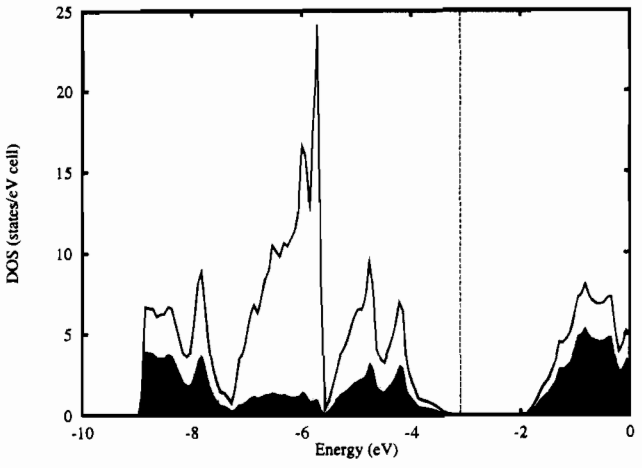

Figure 28. TB–LMTO–ASA *ab initio* density-of-states (DOS) of InBr, with In^+ contributions emphasized in black.

iterated to self-consistency[45] by use of the ASA and a combined correction term, employing muffin-tin spheres expanded to overlapping and volume filling spheres.

A comparison of one-electron exchange integrals H_{ii} and corresponding many-electron band centers C for InBr is given in Table 3. A naive one-to-one correspondence may not be expected (especially considering the *very* different basis sets); nevertheless the trends are clear: Regardless of the (physically unimportant) relative zeros of both scales,[46] the bromine 4s–4p separation is practically the same (about 12.7 eV). The indium 5s lies below the bromine 4p level in both calculations (0.8 eV in EH, 2.8 eV in LMTO). Most importantly, the indium 5s–5p separation is large (4.7 eV in EH, 9.1 eV in LMTO), the *ab initio* method actually having converged to a larger 5s–5p gap. In other words, the (very small) indium s–p mixing observed in the semiempirical calculations may be safely regarded as an *upper limit* and the (almost insignificant) p participation is more likely to be overestimated than underestimated.

Because of the approximate energetic coincidence between both strongly different methods, an *ab initio* DOS of InBr with indium contributions emphasized in black (Figure 28) is almost *superimposable* in shape with the semiempirical DOS (refer to Figure 14). The only real differences are the slightly larger dispersion of the Br 4p-dominated block (typical for EH theory's overestimation of covalency) and the sizes of the band gap, the latter reflecting the imperfect treatment of electron correlation both in EH theory and in LMTO theory (due to the failure of the local-density approximation).

Supplementary Material Available: Tables of atomic positions, formal valences, quantum mechanical charges, and charge-iterated exchange integrals of all binary indium bromides (5 pages). Ordering information is given on any current masthead page.

(45) Program TB-LMTO by M. van Schilfgaarde, T. A. Paxton, O. Jepsen, and O. K. Andersen.

(46) The difference in energy zeros is completely irrelevant for such calculations having used Bloch's theorem. Upon assuming cyclic boundary conditions, there is no contact to the vacuum level.